

Modelling of a Coil Steam Generator for CSP applications[☆]

Leonardo Pelagotti^a, Kim Sørensen^{b,1}, Thomas J. Condra^b, Alessandro Franco^a

^aEnergy Engineering Department, School of Engineering, Pisa University, Via Diotisalvi 2, 56126 Pisa, Italy

^bDepartment of Energy Technology, Aalborg University, Pontopidanstræde 101, 9200 Aalborg, Denmark

Abstract

The project investigates a new design for a CSP plant steam generation system, the Coil Steam Generator (CSG). This system allows faster start-ups and therefore higher daily energy production from the Sun. An analytical thermodynamic simulation model of the evaporator and a mechanical analysis are developed to optimize the behavior of the system in different start-up scenarios. The results improve the effective life time (ELT) of the CSG, the thermal flexibility of the overall CSP plant to have faster start-ups. Sensitivity analysis carried out to understand the importance of start-up time, oil circuit pressure in the CSP plant and header thickness, show that these variables are important to determine the total state of stress in the headers, and therefore their effective life time. Applying the results of the optimization analysis means that, the oil headers are not critical anymore regarding the start-up process and can easily resist faster start-ups.

Keywords: CSP, Evaporator, Effective Life Time, Start-up, Solar Energy

2010 MSC: 00-01, 99-00

1. Introduction

Why is Solar Energy interesting? There is a high potential of development of the use of (CSP) technology; the Sun is the renewable source on which there is the highest possibility to rely on in the future, in fact in one year the solar energy reaching the earth is about twice as much as will ever be obtained from all of the Earth's non-renewable resources.[1]

The CSP technology is complementary to the solar photovoltaic (PV) process. It uses concentrating collectors to provide high temperature heat, usually to a conventional steam power cycle. Efficient and low-cost thermal energy storage technologies can be integrated into CSP systems, allowing electricity production according to the demand profile. CSP systems can also avoid *shadow plant capacity* needed to secure generation capacity in periods without sunshine, can provide grid services, and if desired even black start capabilities. It thus supports the penetration of a high share of intermittent renewable sources like wind or PV and avoids

a high share of expensive electric storage technology in the grid systems. CSP focuses on two technology options: *parabolic trough* technologies and *solar tower* technologies [2]. The CSG investigated in this paper is part of the parabolic trough technology, that is the most mature and economic solar thermal power generation technology today. Solar radiation is concentrated by parabolically curved, trough-shaped reflectors onto a receiver pipe running along the inside of the curved surface. Within the pipe, the solar energy heats up a heat transfer medium (*e.g.* oils, molten salt) to approximately 400°C. The medium transfers the heat to a power block, where steam is generated and electricity is produced in a conventional Rankine cycle.

By its unsteady nature, both within the day and the year, the capture and storage of solar energy is critical if a significant portion of the total energy demand needs to be met by this renewable form of energy. Fast start-ups and higher plant flexibility are necessary to extract as much power as possible from the Sun in CSP plants, in the limited amount of hours of solar radiation in a day. This is why a study on the thermal flexibility of CSP plants is of enormous importance to guarantee, in the near future, an increasing percentage of solar energy from

[☆]This document is a collaborative effort between Pisa University and Aalborg University with Aalborg CSP A/S.

¹Corresponding Author, kso@et.aau.dk

CSP technology. The electricity grid requires the thermal plants to be as fast as possible to be able to supply the difference between power production and demand at any time. A system which is capable of providing flexibility to the grid could be a CSP power plant with a daily heat storage system based on molten salts or a steam generator unit where the steam is accumulated in the drum. ²

2. Material and Methods

The coil-type evaporator analyzed in this project, see Figure 1, has been specially developed for solar energy applications, where high steam capacity and high steam pressures are required due to frequent starts/stops and load changes, due to the intermittent nature of the Sun [3].

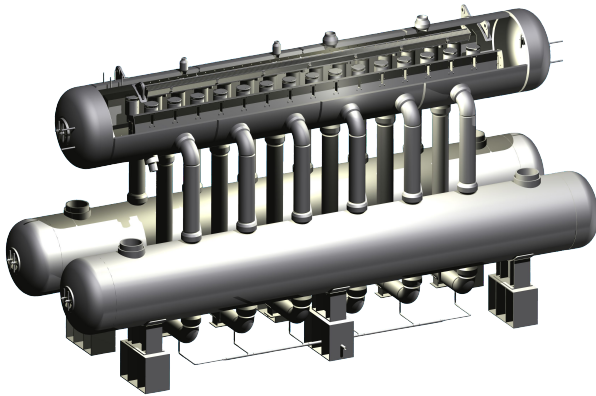


Figure 1: Steam generation system of the CSP plant.[3]

The coil-type evaporator does not have thick tube plates. The hot oil flows are distributed to the heat transfer tube bank via a circular manifold, or oil header as shown in Figure 2. The round shape of the header results in a relatively small material thickness and therefore low thermal stress as can be understood from Equations 11, 12 and 13 where the thermal stress is proportional to the square of the thickness. The new design of the oil collectors as cylindrical headers lowers the thermal stresses that were affecting seriously the life time. Moreover, by

²The author of this Paper have been in cooperation with the engineering company Aalborg CSP A/S, who manufactures heat exchangers for solar applications and develops and supplies steam generators for utility size CSP plants.

splitting the evaporator unit in two heat exchangers and a steam drum, the diameters of the individual pressure vessels are smaller compared to a shell and tube evaporator, and the wall thickness required to sustain the pressure is smaller too. This means that the evaporator is less sensitive to fast temperature gradients and therefore is more flexible. That is exactly why the coil-type steam generator is especially interesting for solar applications that requires faster start-ups.

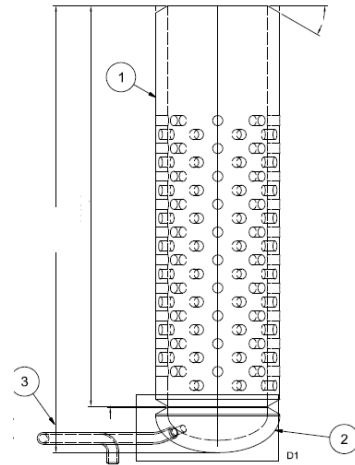


Figure 2: Circular oil header

Thermodynamic Model. The thermodynamic model includes energy balances and several heat transfer correlations, necessary to describe the cross flow evaporation process on the evaporator tube bundle. The data are based on heat balances and plant measurements provided by Aalborg CSP, and the model is solved analytically in MATLAB.

Figure 3 shows how the system has been conceptually described for the development of the Model.

The purpose of this model is to calculate the temperature distributions in the tube bundle of the evaporator, in every point of the 3-D space in the shell and thus determine the temperature in the oil headers. The model is based on the following assumptions: quasi-static conditions, no heat loss, the wall thermal resistance is uniform and negligible longitudinal heat transfer in both wall and fluid.

The model uses the $\epsilon - NTU$ method and solves an analytical system of partial-ordinary differential equations, as shown in Equation 1, from [4]. The system is derived from a 2-D energy balance of the heat exchange process in a cross flow evaporator, and is then made 3-D by the author, invoking the

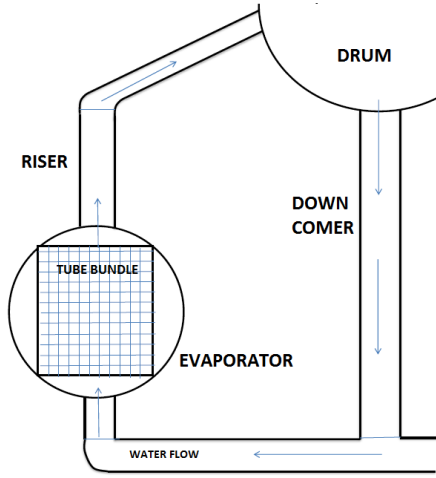


Figure 3: Cross sectional volume discretization principle of the entire tube bundle.

assumption of axial symmetry for the tube in the tube bundle of the cross flow evaporator. The configuration for the cross flow heat exchanger is supposed to be unmixed on the water/steam side and mixed in the thermal oil side. This is due to the discretization used for the evaporator. This results in a 2D dimensional temperature field for the water/steam flow and a 1-D temperature field for the oil flow inside the tube. The model is based on Eq. 1, composed of differential equations, one partial and one ordinary.

$$\begin{cases} \frac{\partial \theta_2}{\partial \xi} + \theta_2 = \theta_1 \\ \frac{d\theta_1}{d\chi} + \theta_1 = \frac{1}{C^* NTU} \cdot \int_0^{C^* NTU} \theta_2 d\xi \end{cases} \quad (1)$$

The system above is made non dimensional and the symbols used are:

$$\theta_1 = \frac{T_1 - T_{2,i}}{T_{1,in} - T_{2,in}} \quad \theta_2 = \frac{T_2 - T_{2,in}}{T_{1,in} - T_{2,in}} \quad (2)$$

$$\chi = \frac{z}{L1} NTU \quad \xi = \frac{y}{L2} C^* NTU \quad (3)$$

The domain is $0 \leq \chi \leq NTU$ and $0 \leq \xi \leq C^* NTU$ and the boundary conditions $\theta_1(0) = 1$ and $\theta_2(\chi, 0) = 0$.

The solution of the above system of equations is carried out analytically implementing and solving in MATLAB. Applying the Laplace and Inverse

Laplace Transform technique and solving the integrals, the results is shown in Eq. 4.

$$\begin{cases} \theta_1(\chi) = e^{-K\chi} \\ \theta_2(\chi, \xi) = (1 - e^{-\xi}) \cdot e^{-(K\chi)} \end{cases} \quad (4)$$

Where K is a parameter related to the NTU method, and 1 refers to the oil and 2 to the water/steam.

$$K = \frac{(1 - \exp^{-C^* NTU})}{C^* NTU} \quad (5)$$

The overall heat transfer coefficient value for UA is evaluated for every sections of the entire tube bundle with Eq. 6.

$$\frac{1}{UA} = \frac{1}{h_{oil} A_i} + \frac{\delta}{k_w A_{mean}} + \frac{1}{h_{w/s} A_o} \quad (6)$$

The heat transfer coefficient for the oil, h_{oil} , is evaluated with the *Second Petukhov equation*, [5]. Instead for calculating the heat transfer coefficient on the water/steam side, it is necessary to use correlations developed for a tube bundle in a horizontal cross flow evaporator, such as the Palen and Yang (1983) correlation or the Thome & Robinson (2006), see [6]. These correlations gives mean bundle boiling heat transfer coefficients and use the h_{NCB} , the *nucleate* boiling heat transfer coefficient and the h_{nc} , the natural convection coefficient of heat transfer around a tube bundle. Several different nucleate boiling correlations have been implemented, such as the Stephan & Abdelsalam [7] and the Ribatski et al. [8] correlation. Additionally a sensitivity analysis on the effect of using different correlations has been also investigated. The h_{nc} , has been calculated using the Zukauskas correlation, see [5].

In order to calculate the enthalpy distribution in the tube bundle from the temperature distribution for every section in the entire evaporator, Eq. 7 has been used to compute the heat flux received by the water/steam on the outside of the tube.

$$\dot{q}(i) = C_{min} (T_{oil}(i+1) - T_{oil}(i)) \quad [W] \quad (7)$$

Assuming that all the heat flux from the oil goes to the water/steam, in order to calculate the enthalpy for every section along the tube diameter, Eq. 8 has been implemented:

$$h_{ws}(i, j + 1) = h_{ws}(i, j) + \left(\frac{nz}{ny} \right) \frac{q(i)}{\dot{m}_{w/s}} \quad \left[\frac{kJ}{kg} \right] \quad (8)$$

Where the i index denotes the tube length coordinate along z and the j index the section on the vertical y coordinate on the tube outside diameter. Also nz and ny is the number of discretization in z and y coordinate. Knowing the value of the enthalpy as a 3D function inside the cross flow evaporator tube bundle, the quality as a 3D space function, assuming thermodynamic equilibrium, is calculated.

It is relevant to understand how the system adapts to different load conditions, and therefore pressure and heat flux ranges. This reflects how the cross flow evaporator works under transient conditions, and that is relevant for a CSP plant. Figure 4 shows the evolution of the exchanged heat flux in the evaporator, during a normal warm start-up of 28 minutes.

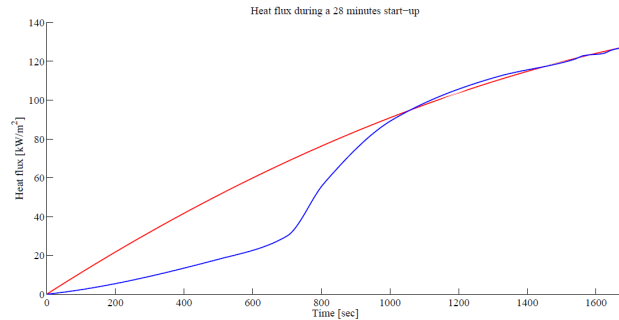


Figure 4: Evolution of the heat flux exchange in the evaporator during a warm start-up of 28 minutes

As it can be seen from Figure 4, the two curves are in good accordance at the end of the start-up phase, when the load is approaching the design value, while instead, the two curves differ significantly at low and medium load cases at the beginning of the start-up. The red curve, with a quadratic shape, represents an interpolate profile based only on the heat flux calculated for high load cases, in a range of 70-100 % of the design load case. The blue curve is the profile based on data from the plant. The fact that the profile at high load cases is different from the profile at lower load cases, means that the evaporator behaves differently according to the load, and that the heat transfer correlations used to describe the system at high loads have to

be different than the ones to use for the lower load cases [9].

3. Theory and Calculations

Thermal-Pressure Stress Analysis. The thermal stresses in the thick walled oil headers are calculated based on the temperature profile, found by solving the heat conduction equation in the wall of the headers. An analytical approach is used for the formulation of the entire problem, involving basic assumptions and the calculation of the temperature in an hollow cylinder in transient conditions, with the Fourier equation of Thermal Conduction applied to the oil header. It is assumed that the problem is symmetrical in the θ coordinate and the final heat equation to be solved is :

$$\frac{1}{r} \frac{\partial}{\partial r} \left(r \frac{\partial T}{\partial r} \right) - \alpha \frac{\partial T}{\partial t} = 0 \quad (9)$$

where α is the thermal diffusivity of the header wall. Eq. 9 is a parabolic partial differential transient equation (PDE). The initial-boundary value problem of parabolic equation in 1-D space and time is given in Eq. 10.

$$\begin{cases} \frac{1}{r} \frac{\partial}{\partial r} \left(r \frac{\partial T}{\partial r} \right) - \alpha \frac{\partial T}{\partial t} = 0 \\ T(r, 0) = T_0 & I.V. \\ T(R_{in}, t) = T_{oil}(t) & B.C. \\ T(R_{out}, t) = T_{w/s}(t) & B.C. \end{cases} \quad (10)$$

Once the temperature in the thickness of the headers is calculated it is possible to calculate the thermal stresses deriving from that profile. The *plane strain state* equations are used in order to compute the thermal stresses, Equations 11 and 12 and 13, as explained in [10] and [11].

$$\sigma_{\theta, th} = \frac{E\alpha}{1-\nu} \frac{1}{r^2} \left[\frac{r^2 + R_i^2}{R_e^2 - R_i^2} \int_{R_i}^{R_e} T(r) r dr + \int_{R_i}^r T(r) r dr - T(r) r^2 \right] \quad (11)$$

$$\sigma_{r, th} = \frac{E\alpha}{1-\nu} \frac{1}{r^2} \left[\frac{r^2 - R_i^2}{R_e^2 - R_i^2} \int_{R_i}^{R_e} T(r) r dr - \int_{R_i}^r T(r) r dr \right] \quad (12)$$

$$\sigma_{z,th} = \frac{E\alpha}{1-\nu} \left[\frac{2}{R_e^2 - R_i^2} \int_{R_i}^{R_e} T(r) r dr - T(r) \right] \quad (13)$$

At the end of the start-up the thermal stresses are shown in Figure 5

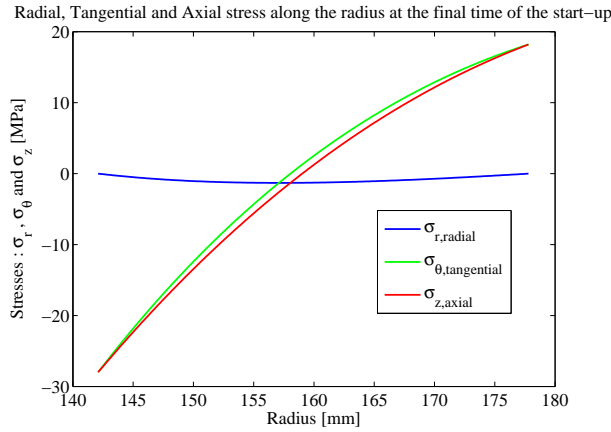


Figure 5: Thermal stresses in the radius at the end of the start-up

Once the thermal stresses are evaluated also the stresses due to the pressure field are considered in Eq. 14, 15 and 16. For a thick walled cylinder the pressure stresses are evaluated with the *Lame Equations*, explained in [12] and [13].

$$\sigma_{r,p}(r) = \frac{P_{in}R_{in}^2 - P_{out}R_{out}^2}{R_{out}^2 - R_{in}^2} + \frac{(P_{out} - P_{in})R_{out}R_{in}^2}{r^2(R_{out}^2 - R_{in}^2)} \quad (14)$$

$$\sigma_{\theta,p}(r) = \frac{P_{in}R_{in}^2 - P_{out}R_{out}^2}{R_{out}^2 - R_{in}^2} - \frac{(P_{out} - P_{in})R_{out}R_{in}^2}{r^2(R_{out}^2 - R_{in}^2)} \quad (15)$$

$$\sigma_{z,p} = 2\nu \left(\frac{P_{in}R_{in}^2 - P_{out}R_{out}^2}{R_{out}^2 - R_{in}^2} \right) \quad (16)$$

The stresses are functions of time and radius and for the design load case at the end of the start-up Figure 6 shows them.

When the stresses are function of time, the failure criteria that has to be applied is the theory of *Fatigue of Material*.

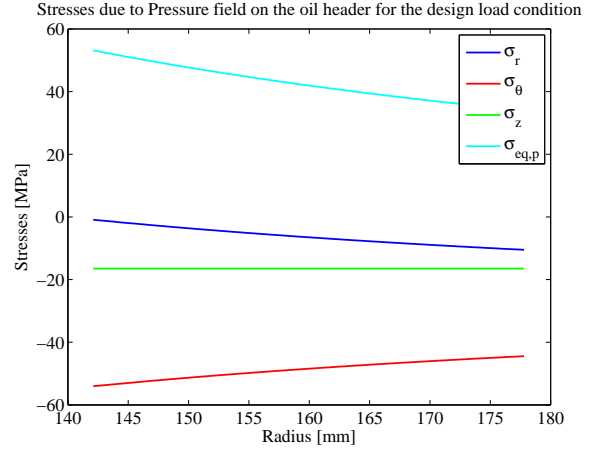


Figure 6: Stresses due to the Pressure field at the design load

Fatigue Analysis. Empirical curves of fatigue endurance have to be applied, but these curves are rarely available, due to the long time required for their estimation. In this project, the *Fatigue Life Evaluation* is carried out using the S-N curves, Basquin law, Goodman diagram and Sines equivalent stress criteria for ductile materials, as explained in [13], [14], [15] and [16].

The first step is to calculate the total transient stress state, caused by the pressure and temperature effect in the header thick-wall. The total stress state is simply the linear superposition of the temperature and pressure derived tension state, as they are independent. Therefore the total radial, tangential and axial stress are calculated as in Equation 17, where $j=r,\theta,z$.

$$\sigma_{j,tot} = \sigma_{j,p} + \sigma_{j,th} \quad (17)$$

At a fixed time, the tension state is expressed in the header by Figure 7.

At the internal radius, where there is the most critical tension state, Figure 8 shows how is the evolution during the time of the total principal stresses. When assuming the start-up as a daily process, followed by the plant shut-down, repeated every day, a repeated alternating stress cycle in the time occurs.

This stress cycle is an alternating cycle with a maximum and minimum stress and a trapezoidal wave form. An holding time between the cycling part of the stress, corresponding to the daily design load at steady state and the night closing down time of the plant is present. The triaxial total state of

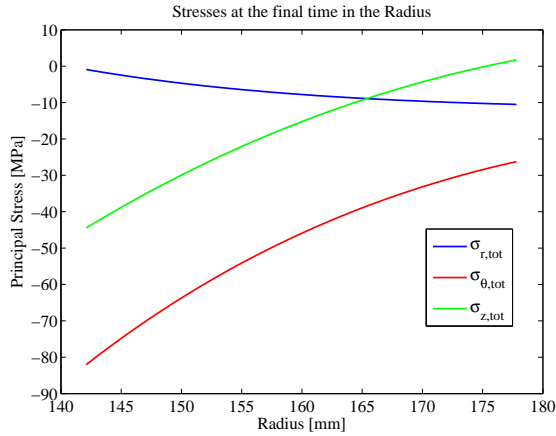


Figure 7: Principal stresses at the design load in the outlet header

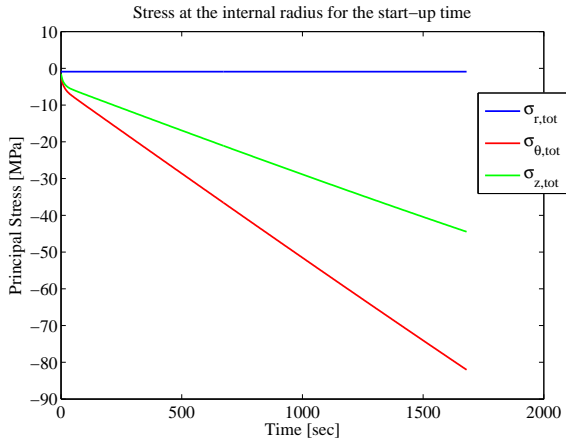


Figure 8: Principal stresses at the internal radius for the start-up time

stress in the time has an alternating component and a mean component of all the three principal stresses as calculated in Eq. 18 and 19 where $j=r,\theta,z$.

$$\sigma_{a,j} = \frac{\sigma_{max,j} - \sigma_{min,j}}{2} \quad (18)$$

$$\sigma_{m,j} = \frac{\sigma_{max,j} + \sigma_{min,j}}{2} \quad (19)$$

Moreover it is important to consider that the applied stresses and fatigue happens at high temperature where it has been proven that there is an interaction between *Creep* and *Fatigue*³.

³But the ASME code [17] suggests to consider creep in

When the nominal *alternating* stresses and nominal *mean* stresses are computed from the alternating cycle, the presence of several holes in the oil header is taken into consideration for calculating the effective stresses. The holes contribute to generate a peak of stress on the surface of the header in the proximity of the hole, that can be calculated using the stress concentration factor K [18]. In fatigue conditions the concentration factor does not apply totally to the intensification of the stress, and the fatigue concentration factor is calculated with the Peterson equation [18].

When the effective stresses are known, an equivalent stress from the triaxial state of stress has to be obtained in order to be able to use the S-N curves necessary for estimating the fatigue life. For cylindrical vessel under triaxial stress state the Sines criteria is used for calculating an equivalent stress, from the three principal effective stresses, [18].

A point corresponding to $\sigma_{a,eq}$ and $\sigma_{m,eq}$ as an equivalent uni-dimensional state of stress in the Goodman diagram is found. The Goodman diagram represents a way of computing an effective pure alternate stress that can be used in the S-N curve (also known as Wöhler curve), from the total state of stress, and is expressed in the Goodman relationship, Eq. 20.

$$\sigma_a = S_N \cdot \left(1 - \frac{\sigma_m}{\sigma_{yield}}\right) \quad (20)$$

S_N is then used in the Wöhler curve to calculate N , the number of cycle before rupture. In order to calculate the S-N curve for the oil header, the Basquin law it is used combined with the Marin formulation, [16].

4. Results

For the specific case of this project, assuming a start-up procedure that follows the maximum allowable thermal gradient in the drum of the CSP plant of 5 K/min from the morning conditions, the warm start-up takes approximately 28 min. For this procedure for the case of the outlet oil header the number of cycles to rupture was calculated to be approx. $N = 5700$, that corresponds to approx.

SA 106 B, the steel of the oil header, only above 370°C, that is actually the maximum temperature at the design load case for the oil. Therefore creep is not considered.

16 years (if a warm start-up is considered every day of the year). If a faster start-up procedure is followed, the same analysis can be carried out. New temperature profiles during time are calculated and different thermal stresses occurs. This results in a different fatigue damage that can be calculated related to how fast the start-up is. Thus a number of cycle to rupture, following the faster start-up is calculated for the outlet oil header as showed in Table 4. It can be seen how having faster a start-up is more critical for the component.

Table 1: Start-up time and corresponding fatigue life

Gradient followed	Start-up time [min]	Fatigue life [years]
3 K/min	47	6800 cycles \approx 19
5 K/min	28	5700 cycles \approx 16
7 K/min	20	4600 cycles \approx 13

5. Discussion and Optimization

A sensitivity analysis on the influence of the oil circuit pressure was carried out. The oil pressure was varied in a feasible range, compared to the CSP plant operational parameters, and Figure 9 summarizes the results. It can be seen from Figure 9 that the life time of the header is highly influenced by the oil circuit pressure. An increasing oil pressure leads to longer fatigue lives. For example if the oil pressure is changed from 10 bar to 100 bar there is an improvement of the fatigue life by a factor of five. This is due to the pressure state of stress that is opposite to the temperature state of stress, and therefore the resultant state of stress is lower, and induces a smaller fatigue damage.⁴

The thickness of the oil header is also a key parameter and highly affects the value of the pressure and thermal stresses. It is easy to understand analyzing Equations 11, 12 and 13 for the thermal stresses in plane strain and Equations 14, 15 and 16 for the pressure stresses. Once a range of feasible values in which varying the thickness is found, the

⁴ Of course the oil circuit pressure modification from 10 bar to 100 bar, has to be thoroughly investigated when applied to all the components of the oil circuit. It has to be a value that does not exceed other limits for other part of the plant. The value of 100 bar is an tentative value that expresses the high influence of the oil circuit pressure on the effective life of the oil headers.

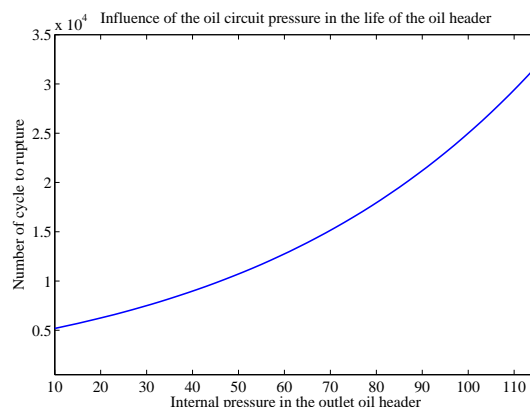


Figure 9: Influence of the oil pressure in the fatigue life of the Outlet Header for a start-up of 20 min

sensitivity analysis can be carried out for what concerns the thickness. Varying the thickness value for the outlet header and repeating the fatigue life calculation for each value, Figure 10 was found. There is an optimum in the value of the thickness at fixed R_{in} that gives a maximum fatigue life of the component with the right thickness value. The optimum depends on the thermal and pressure stresses and therefore on the start-up time and scenarios. It is therefore interesting at the design phase to take into account the thickness value as a parameter affecting the effective life of the header. The faster is the start-up and the lower is the thickness optimum value as shown in Table 2.

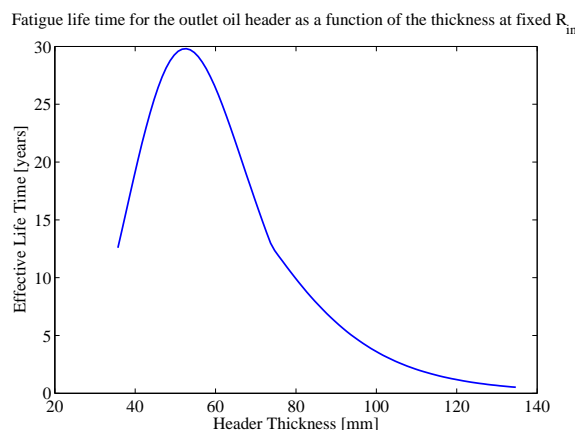


Figure 10: Fatigue Life for the Outlet Header as a function of the header thickness

This is because the thickness value is influenced with an upper limit from the thermal stresses. The higher the thermal stresses are and the lower is

Table 2: Optimized outlet header thickness

Start-up time	Optimum thickness
15 minutes	47 mm
20 minutes	53 mm
28 minutes	58 mm

the upper limit value on the header thickness. So faster start-up, means higher thermal stresses and lower optimum thickness of the header. Table 5 summarizes the main results and the optimizations. WSU20 stands for a warm start-up that takes 20 minutes. WSU20OHT is the WSU20 scenario with the optimum header thickness value.

Table 3: Main results of the Analysis on the Effective Life Time of the Outlet Oil Header

Scenarios	ELT [years]
WSU20	13
WSU28	16
WSU47	19
WSU20 & 100 bar oil pressure	68
WSU20OHT	29
WSU20OHT & 100 bar oil pressure	90
WSU20 & oil pressure \equiv drum pressure	≥ 100
WSU10 & overall optimization	25

Another way to optimize the oil circuit pressure is finding the best oil pressure profile as a function of time during the start-up. It was found that a oil pressure profile that follows the drum pressure building-up during the start-up is a very good strategy in order to drastically reduce the pressure stresses in the header and therefore the total state of tension. Since the pressure in the system is high, also the stresses related are significant. Reducing them, means reduce an high component of the state of tension. In fact the outlet header for a start-up of 20 minutes, that has a calculated ELT of approximately 13 years, reaches a calculated ELT of more than 100 years if the oil pressure follows exactly the drum pressure at any time during the start-up. See Table 5 .

6. Conclusions

Using the thermodynamic model developed for the tube bundle in the evaporator it was possible to predict the behavior of the evaporation process

inside the tube bundle for different load conditions, and also the behavior of several variables with accuracy in the 3D space inside the shell of the evaporator. Knowing the temperature in the evaporator, and using a quasi-static stress analysis it was possible to investigate the oil headers and understand how they react to different loads and scenarios. Results show that not only the thermal stresses are significant but also the pressure stresses have to be considered.

When the stresses are calculated for different load cases, using a fatigue life calculation method it was possible to study the effect on the life of the oil headers for different start-up procedures. Several sensitivity analysis were carried out on the importance of start-up time, oil circuit pressure and header thickness.

It was found that the value of the oil circuit pressure is extremely important on determining the total state of stress in the headers, and therefore their effective life time. If the right value of the pressure is used in the CSP plant, the effective fatigue life can be increased significantly. This means that the headers would not be a critical component for the plant anymore, regarding the start-up procedure, and this would make a faster start-up possible. Also the value of the thickness of the header is very important and can lead to significant improvement of the effective life time. If the thickness is increased from 36 mm to the optimum value the life is increased up to more than double.

Having a 10 minutes faster start-up in the morning of one CSP plants of 75 MW, leads to an energy production higher of 12.5 MWh every day and more than 4500 MWh_{el} a year. This means that, if there are 6 CSP plants of 75 MW each run by a Company, the annual income would be approximately 1 Million dollars higher ⁵. With the study developed it was indeed possible to find the right design value for several parameters in order to increase the effective life of the system and therefore be able to have a several minutes faster start-up.

A Analysis of the same kind can be applied to similar systems in thermal power plants of different kinds, in order to improve their flexibility regarding transient conditions. This means moving towards the possibility to increase the share of renewable and unpredictable energy sources in the electricity grid.

⁵Considering 40\$/MWh as the price of the produced electricity.

Nomenclature

Symbol	Name	Unit
α	Thermal diffusivity	m^2/s
α	Coefficient of linear thermal expansion	K^{-1}
A	Area	m^2
C	Flow Stream Heat Capacity	$W/K, \%$
χ	A-dimensional length along z	—
E	Young Module	GPa
h	Heat transfer coefficient	W/m^2K
k	Thermal conductivity	W/mK
K	NTU constant	—
$L1$	Longitudinal dimension along z	m
$L2$	Vertical Dimension along y	m
m	Mass flow	kg/s
NTU	Number of transfer unit	—
ν	Poisson Module	—
P	Pressure	bar
q	Heat flux	W/m^2
r	radius	mm
R	radius	mm
S	Stress	MPa
σ	Stress	MPa
t	Time	sec
T	Temperature	C, K
U	Overall heat transfer coefficient	W/m^2K
θ	A-dimensional Temperature	—
ξ	A-dimensional length along y	—
y	Vertical coordinate	m
z	Longitudinal coordinate	m

Subscript

1	Oil
1	Water
a	Alternate
e	External
i	Internal
in	Inlet
m	Mean
max	Max
$mean$	Mean
min	Min
N	Number of cycle
o	External
oil	Oil
out	Outlet
p	Pressure
r	Radial
th	Thermal
θ	Tangential
w	Wall
w/s	Water/steam
$yield$	Yield
z	Axial
*	Min/Max Ratio

References

- [1] Joint-Research-Centre, Solar radiation, Website, last checked: 5.06.2014 (2014).
URL <http://re.jrc.ec.europa.eu>
- [2] SBC, Economic opportunities resulting from a global deployment of concentrated solar power (csp) technologies, Energy Police.
- [3] AalborgCSP, Aalborg csp, Website, last checked: 5.06.2014 (2014).
URL <http://www.aalborgcsp.com/>
- [4] R. K. Shah, D. Sekulic, Fundamentals of heat exchanger design, 1st Edition, Wiley India, 2003, iSBN-10: 0471321710.
- [5] Y. A. Cengel, J. Ghajar, Heat and Mass Transfer, 4th Edition, Mc Graw Hill, 2011.
- [6] J. G. Collier, J. R. Thome, Convective boiling and condensation, 3rd Edition, Oxford University Press, 1994, iSBN: 0191591262.
- [7] K. Stephan, M. Abdelsalam, Heattransfer correlations for natural convection boiling., International Journal of Heat and Mass Transfer, 23(1):7387.
- [8] R. G., S. J. J. M., da Silva E. F., Modeling and experimental study of nucleate boiling on a vertical array of horizontal plain tubes., Experimental Thermal and Fluid Science, 32(8):15301537.
- [9] A. Franco, Conversations and courses material, Conversation at Pisa University.
- [10] R. F. Barron, B. R. Barron, Design for Thermal Stresses, 1st Edition, Wiley, 2011, iSBN: 978-0-470-62769-3.
- [11] A.Kandil, A. El-Kady, A. El-Kafrawy, Transient thermal stress analysis for thick-walled cylinder, Int. J. Mech. Sci. Vol. 37, No. 7, pp. 721-732, 1995.
- [12] J. M. Gere, S. P. Timoshenko, Mechanics of Materials, 5th Edition, PWS Kent Publishing, 1970.
- [13] P. Forte, Conversation and courses material and lectures, Master in Energy Engineering at Pisa University.
- [14] R. C. Juvinall, K. M. Marsheck, Fondamenti della progettazione dei componenti nelle macchine, 1st Edition, Edizioni ETS, 2001, iSBN :88-7741-730-7.
- [15] R. Hetnarski, M. Eslami, Thermal Stresses- Advanced Theory and Applications, 1st Edition, Springer, 2009, iSBN 978-1-4020-9246-6.
- [16] R. Budynas, J. Nisbett, Shigley's Mechanical Engineering Design, 9th Edition, Mc Graw Hill, 2010, iSBN-10: 0077942906.
- [17] ASME, ASME Boiler and Pressure Vessel Code (BPVC) — 2013 (2013).
- [18] A. D. Paulis, E. Manfredi, Costruzione di Macchine, 1st Edition, Pearson, 2012, iSBN : 978-88-7192-783-1.